Journal of Computational Physics 227 (2008) 8489–8507

Contents lists available at ScienceDirect

Journal of Computational Physics

journal homepage: www.elsevier.com/locate/jcp

Numerical computations for long-wave short-wave interaction equations in semi-classical limit

Qianshun Chang [a], Yau-Shu Wong [b,*], Chi-Kun Lin [c]

[a] Institute of Applied Mathematics, Academy of Mathematics and System Science, The Chinese Academy of Sciences, Beijing 100080, China
[b] Department of Mathematical and Statistical Sciences, University of Alberta, Edmonton, Canada T6G 2G1
[c] Department of Applied Mathematics, National Chiao Tung University, Hsinchu 30010, Taiwan

ARTICLE INFO

Article history:
Received 11 September 2007
Received in revised form 14 May 2008
Accepted 16 May 2008
Available online 5 June 2008

Keywords:
Numerical methods
Finite-difference schemes
Long-wave short-wave interaction equations
Semi-classical limit

ABSTRACT

This paper presents and compares various numerical techniques for the long-wave short-wave interaction equations. In addition to the standard explicit, implicit schemes and the spectral methods, a novel scheme SRK which is based on a time-splitting approach combined with the Runge–Kutta method is presented. We demonstrate that not only the SRK scheme is efficient compared to the split step spectral methods, but it can apply directly to problems with general boundary conditions. The conservation properties of the numerical schemes are discussed. Numerical simulations are reported for case studies with different types of initial data. The present study enhances our understanding of the behavior of nonlinear dispersive waves in the semi-classical limit.

1. Introduction

In this paper, we study the long-wave short-wave interaction equations

$$\mathrm{i}\epsilon\psi_t^\epsilon + \frac{\epsilon^2}{2}\psi_{xx}^\epsilon - (\alpha(|\psi^\epsilon|^2 - 1) + V^\varepsilon)\psi^\epsilon = 0, \tag{1.1}$$

$$V_t^\varepsilon = -\lambda(|\psi^\epsilon|^2)_x, \tag{1.2}$$

where the complex-valued function ψ^ϵ and the real-valued function V^ϵ represent the envelope of the short-wave and the amplitude of the long-wave, respectively. The parameter ϵ is analogous to the Planck constant. The coupling between the long-wave and short-wave is given by λ, which is real and introduces the dispersion interaction. The nonlinearity in the coupled system is due to α. $\alpha > 0$ corresponds to the defocusing nonlinearity, and $\alpha < 0$ represents the focusing nonlinearity. However, due to the hydrodynamical structure, we only discuss the defocusing case in this paper. The initial values are given by

$$\psi^\epsilon(x,0) = \psi_0^\epsilon(x), \tag{1.3}$$

$$V^\epsilon(x,0) = V_0^\epsilon(x). \tag{1.4}$$

The water wave interaction equations (1.1)–(1.4) has been used to model surface waves in the presence of both gravity and capillary modes. The topic is also of interest in plasma physics [23]. The equations can be derived as the substitute for the Davey–Stewartson system due to the effect of resonance, a phenomenon that occurs when the group velocity of the short

* Corresponding author. Tel.: +1 780 492 4376; fax: +1 780 492 6826.
E-mail addresses: qschang@amss.ac.cn (Q. Chang), yaushu.wong@ualberta.ca (Y.-S. Wong), cklin@math.nctu.edu.tw (C.-K. Lin).

0021-9991/$ - see front matter © 2008 Elsevier Inc. All rights reserved.
doi:10.1016/j.jcp.2008.05.015

waves matches the phase velocity of the long waves [7,15]. When $V^\epsilon = 0$, Eq. (1.1) is a nonlinear Schrödinger (NLS) equation which has been studied by many mathematicians and physicists. If $\lambda = 0$, Eq. (1.1) is the cubic NLS equation with a stationary potential $V^\epsilon = V_0^\epsilon(x)$. Integrating Eq. (1.2) in t and eliminating V^ϵ in Eq. (1.1), the system can be rewritten as

$$\mathrm{i}\epsilon\psi_t^\epsilon + \frac{\epsilon^2}{2}\psi_{xx}^\epsilon = -\lambda\left[\int_0^t (|\psi^\epsilon(x,\tau)|^2)_x \,\mathrm{d}\tau\right]\psi^\epsilon + [V_0^\epsilon(x) + \alpha(|\psi^\epsilon|^2 - 1)]\psi^\epsilon, \quad \psi^\epsilon(x,0) = \psi_0^\epsilon(x).$$

In [23], Ogawa proved the global well-posedness of Eqs. (1.1)–(1.4) for $\epsilon = 1$ in the largest class of the initial data. Let bar "-" denote the complex conjugate. Through a direct deduction, the following conservation laws can be obtained:

$$\int_{-\infty}^{\infty} |\psi^\epsilon(x,t)|^2 \,\mathrm{d}x = \text{const.}, \tag{1.5}$$

$$\int_{-\infty}^{\infty} \frac{\mathrm{i}\epsilon}{2}\left(\frac{\overline{\psi_x^\epsilon(x,t)}}{\overline{\psi^\epsilon(x,t)}} - \frac{\psi_x^\epsilon(x,t)}{\psi^\epsilon(x,t)}\right)\mathrm{d}x = \text{const.}, \tag{1.6}$$

$$\int_{-\infty}^{\infty} V^\epsilon(x,t)\,\mathrm{d}x = \text{const.}, \tag{1.7}$$

$$\int_{-\infty}^{\infty} \left[\frac{\mathrm{i}\epsilon}{2}(\psi^\epsilon(x,t)\overline{\psi_x^\epsilon(x,t)} - \psi_x^\epsilon(x,t)\overline{\psi^\epsilon(x,t)}) + \frac{1}{2\lambda}|V^\epsilon(x,t)|^2\right]\mathrm{d}x = \text{const.}, \tag{1.8}$$

$$\int_{-\infty}^{\infty} V_t^\epsilon(x,t)|\psi^\epsilon(x,t)|^2\,\mathrm{d}x = 0, \tag{1.9}$$

$$\int_{-\infty}^{\infty} E^\epsilon(x,t)\,\mathrm{d}x = \text{const.}, \tag{1.10}$$

where the energy density E^ϵ is given by

$$E^\epsilon(x,t) = \frac{\epsilon^2}{2}|\psi_x^\epsilon(x,t)|^2 + \frac{\alpha}{2}(|\psi^\epsilon(x,t)|^2 - 1)^2 + V^\epsilon(x,t)|\psi^\epsilon(x,t)|^2. \tag{1.11}$$

The semi-classical problem has been the subject of research in the past 20 years (see [3,8,13,14,18–22]). Recently, considerable interest has been reported on the semi-classical limit of the water wave interaction equations since the study enhances our understanding of the general semi-classical behavior of the nonlinear dispersive waves. There are many works related to the numerical study of the semi-classical limit of the nonlinear Schrödinger equation. In [2,3] Bao et al. investigate the performance of time-splitting spectral approximations for general nonlinear Schrödinger equations in semi-classical regimes (see also [5]). The Wigner measure approach for the Dufort–Frankel difference scheme is reported in [21]. Markowich et al. in [20] discuss a similar problem using the semi-classical differential Weyl operator with a smooth symbol.

Even though numerous computational methods have been investigated for the single nonlinear equation (see [2–5,9–27]); to the best of our knowledge, numerical simulation for the coupled system given in (1.1)–(1.4) has not been reported. The purpose of this work is to present numerical methods which are capable of solving the coupled system of interaction equations. For the model problem, we consider $x \in [x_L, x_R]$, $t \geqslant 0$, and with the following periodic boundary condition:

$$\psi^\epsilon(x_L,t) = \psi^\epsilon(x_R,t). \tag{1.12}$$

However, other boundary conditions such as the Dirichlet or Neumann types could be imposed.

In the remainder of the paper, we consider various numerical algorithms for the solutions of Eqs. (1.1)–(1.4) and (1.12). Since the mathematical problem admits certain conservation laws, and we will prove that some of the conservative properties are preserved in the numerical schemes. To assess the accuracy and effectiveness of the computational schemes, numerical simulations are preformed for various test cases including particular cases corresponding to the plane wave and soliton in which exact solutions are known.

2. Numerical schemes

We now present various numerical schemes for the solutions of the long-wave short-wave interaction equations given in Eqs. (1.1)–(1.4) with a periodic boundary condition Eq. (1.12). First, the following notations are defined:

$$\begin{aligned}
&x_j = x_L + jh, \quad t^n = n\cdot\tau, && 0 \leqslant j \leqslant J = \left[\tfrac{x_R - x_L}{h}\right], \quad n = 0,1,2,\ldots,\left[\tfrac{T}{\tau}\right],\\
&\psi^\epsilon(j,n) \equiv \psi^\epsilon(x_j,t^n), && V^\epsilon(j,n) \equiv V^\epsilon(x_j,t^n),\\
&\psi_j^n \sim \psi^\epsilon(j,n), && V_j^{n+\frac{1}{2}} \sim V^\epsilon(x_j,(n+\tfrac{1}{2})\tau),\\
&(W_j^n)_x = \tfrac{1}{h}(W_{j+1}^n - W_j^n), && (W_j^n)_{\bar{x}} = \tfrac{1}{h}(W_j^n - W_{j-1}^n),\\
&(W_j^n)_t = \tfrac{1}{\tau}(W_j^{n+1} - W_j^n), && r \equiv \tfrac{\tau}{h^2}, \quad s \equiv \tfrac{\tau}{h},\\
&\|W^n\|_2^2 = h\sum_{j=1}^{J}|W_j^n|^2, && \|W^n\|_\infty = \sup_{1\leqslant j\leqslant J}|W_j^n|.
\end{aligned}$$

2.1. Crank–Nicolson implicit (CNI) scheme

The CNI is a well-known implicit method which has been widely used in numerical analysis. The CNI scheme is given by

$$\mathrm{i}\epsilon(\psi_j^n)_t + \frac{\epsilon^2}{4}(\psi_j^{n+1} + \psi_j^n)_{x\bar{x}} - \left(\alpha\left(\frac{|\psi_j^{n+1}|^2 + |\psi_j^n|^2}{2} - 1\right) + V_j^{n+\frac{1}{2}}\right)\frac{\psi_j^{n+1} + \psi_j^n}{2} = 0, \tag{2.1}$$

$$(V^{n-\frac{1}{2}})_t = -\lambda\frac{|\psi_{j+1}^n|^2 - |\psi_{j-1}^n|^2}{2h}, \tag{2.2}$$

$$\psi_j^0 = \psi_0^\epsilon(x_j), \tag{2.3}$$

$$V_j^{-\frac{1}{2}} = V_0^\epsilon(x_j), \tag{2.4}$$

$$\psi_j^n = \psi_{J+j}^n, \qquad n = 1, 2, \ldots, 1 \leqslant j \leqslant J \tag{2.5}$$

Note that, Eq. (2.1) is implicit and the solution requires solving a tridiagonal system of nonlinear equations. However, Eq. (2.2) is explicit and the unknowns $V_j^{n+\frac{1}{2}}$ can be computed directly. To solve Eq. (2.1), the following simple iterative algorithm can be employed

$$\begin{aligned}&\frac{\epsilon^2 r}{4}\psi_{j+1}^{n+1(s+1)} + \left[\mathrm{i}\epsilon - \frac{\epsilon^2 r}{2} - \frac{\tau}{2}\left(\alpha\left(\frac{|\psi_j^{n+1(s)}|^2 + |\psi_j^n|^2}{2} - 1\right) + V_j^{n+\frac{1}{2}}\right)\right]\psi_j^{n+1(s+1)} \\ &\quad = -\frac{\epsilon^2 r}{4}\psi_{j-1}^{n+1(s+1)} - \frac{\epsilon^2 r}{4}\psi_{j+1}^n + + \left[\mathrm{i}\epsilon + \frac{\epsilon^2 r}{2} + \frac{\tau}{2}\left(\alpha\left(\frac{|\psi_j^{n+1(s)}|^2 + |\psi_j^n|^2}{2} - 1\right) + V_j^{n+\frac{1}{2}}\right)\right]\psi_j^n - \frac{\epsilon^2 r}{4}\psi_{j-1}^n,\end{aligned} \tag{2.6}$$

where the superscript s denotes the s-th iterate in solving the nonlinear equations at a given time step. The initial iterate $\psi_j^{n+1(0)}$ can be chosen as

$$\psi_j^{n+1(0)} = \psi_j^n.$$

Hence, the resulting tridiagonal system Eq. (2.6) can be computed by the standard Gaussian elimination method. The iteration continues until the condition

$$\max_j |\psi_j^{n+1(s+1)} - \psi_j^{n+1(s)}| < 10^{-6} \tag{2.7}$$

is reached. The truncation error of the CNI scheme is of order $O(\tau^2 + h^2)$. According to the linearized stability analysis, the CNI scheme is unconditionally stable.

2.2. Three-level explicit (3LE) scheme

In order to eliminate the requirement to solve nonlinear difference equations, we consider two explicit schemes. The first method is based on the 3LE algorithm

$$\mathrm{i}\epsilon\frac{\psi_j^{n+1} - \psi_j^{n-1}}{2\tau} + \frac{\epsilon^2}{2}(\psi_j^n)_{x\bar{x}} - \left(\alpha(|\psi_j^n|^2 - 1) + V_j^{n+\frac{1}{2}}\right)\psi_j^n = 0, \tag{2.8}$$

$$(V_j^{n-\frac{1}{2}})_t = -\lambda\frac{|\psi_{j+1}^n|^2 - |\psi_{j-1}^n|^2}{2h}. \tag{2.9}$$

The truncation error of the 3LE scheme is of order $O(\tau^2 + h^2)$. According to the linearized stability analysis, the 3LE is conditionally stable if $\frac{\tau\epsilon}{h^2} \leqslant \frac{1}{2}$.

2.3. Hopscotch (HOP) scheme

Another explicit scheme is given by HOP, where Eq. (1.1) is solved in two steps. First, an explicit step

$$\mathrm{i}\epsilon(\psi_j^n)_t + \frac{\epsilon^2}{2}(\psi_j^n)_{x\bar{x}} - \left(\alpha(\frac{|\psi_{j+1}^n|^2 + |\psi_{j-1}^n|^2}{2} - 1) + V_j^{n+\frac{1}{2}}\right)\psi_j^n = 0, \tag{2.10}$$

is used for the odd values of $n + j$; then an implicit step

$$\mathrm{i}\epsilon(\psi_j^n)_t + \frac{\epsilon^2}{2}(\psi_j^{n+1})_{x\bar{x}} - \left(\alpha(\frac{|\psi_{j+1}^{n+1}|^2 + |\psi_{j-1}^{n+1}|^2}{2} - 1) + V_j^{n+\frac{1}{2}}\right)\psi_j^{n+1} = 0, \tag{2.11}$$

is applied for the even values of $n+j$. Notice that, ψ_j^{n+1} are computed explicitly by Eq. (2.10). Although Eq. (2.11) is expressed in an implicit form, since the values ψ_j^{n+1} when $n+j$ odd are already known, it is actually an explicit formula for ψ_j^{n+1} when $n+j$ is even. Combining Eqs. (2.10) and (2.11), Eq. (2.10) may be replaced by the extrapolation formula

$$\psi_j^{n+1} = 2\psi_j^n - \psi_j^{n-1}, \tag{2.12}$$

for odd values of $n+j$. The solution for V is given by

$$(V_j^{n-\frac{1}{2}})_t = -\lambda \frac{|\psi_{j+1}^n|^2 - |\psi_{j-1}^n|^2}{2h}. \tag{2.13}$$

The truncation error for the HOP scheme is of order $O\left(\tau^2 + h^2 + \frac{\tau^2}{h^2}\right)$. Therefore, the condition $\tau = o(h)$ is required to ensure the convergence. Unlike the 3LE scheme, the HOP is unconditionally stable by means of the linearized stability analysis.

2.4. Split step spectral (SSS) method

The SSS is similar to the scheme proposed by Taha and Ablowitz in [25], in which Eq. (1.1) is split into two equations at a given time step as follows:

$$\mathrm{i}\epsilon\psi_t^\epsilon = -\frac{\epsilon^2}{2}\psi_{xx}^\epsilon, \tag{2.14}$$

and

$$\mathrm{i}\epsilon\psi_t^\epsilon = (\alpha(|\psi^\epsilon|^2 - 1) + V^\epsilon)\psi^\epsilon. \tag{2.15}$$

The first equation is a linear partial differential equation which can be solved exactly by the Fourier method, and the second is an ordinary differential equation. The SSS scheme is given by

$$\widetilde{\psi}_j^{n+1} = \mathrm{e}^{-\frac{\mathrm{i}\tau}{\epsilon}\left(\alpha\left(|\psi_j^n|^2-1\right)+V_j^{n+\frac{1}{2}}\right)} \times \psi_j^n, \tag{2.16}$$

$$\psi_j^{n+1} = F_j^{-1}\left(\mathrm{e}^{-\mathrm{i}\tau\epsilon k^2\pi^2/2p^2} \times F_k\left(\widetilde{\psi}_j^{n+1}\right)\right), \tag{2.17}$$

$$\left(V_j^{n-\frac{1}{2}}\right)_t = -\lambda \frac{|\psi_{j+1}^n|^2 - |\psi_{j-1}^n|^2}{2h}, \tag{2.18}$$

where p is half of the space interval $[x_L, x_R]$ and F_k denotes a discrete Fourier transform. The SSS has a high accuracy, and the truncation error is of order $(\tau^2 + h^m)$ where m denotes the smoothness of the solution. Using the linearized stability analysis, we show that the SSS scheme is unconditionally stable.

2.5. Split step Runge–Kutta (SRK) method

The Runge–Kutta scheme is a well-known numerical algorithm for solving differential equations. In the proposed SRK method, we first apply the five-point difference scheme to discretize the term $\frac{\epsilon^2}{2}\psi_{xx}^\epsilon$ in Eq. (2.14), the resulting difference equations are then solved by the fourth-order Runge–Kutta method. The SRK scheme is given as follows:

$$\widetilde{\psi}_j^{n+1} = \mathrm{e}^{-\frac{\mathrm{i}\tau}{\epsilon}\left(\alpha\left(|\psi_j^n|^2-1\right)+V_j^{n+\frac{1}{2}}\right)} \times \psi_j^n, \tag{2.19}$$

$$\psi_j^{n+1} = \widetilde{\psi}_j^{n+1} + (K_1 + 2K_2 + 2K_3 + K_4)/6, \tag{2.20}$$

$$K_1 = G(\widetilde{\psi}_j^{n+1}), \qquad K_2 = G(\widetilde{\psi}_j^{n+1} + 0.5K_1),$$

$$K_3 = G(\widetilde{\psi}_j^{n+1} + 0.5K_2), \qquad K_4 = G(\widetilde{\psi}_j^{n+1} + K_3),$$

$$G(\eta_j^n) = \frac{\mathrm{i}\epsilon\tau}{2h^2}(-\eta_{j+2}^n/12 + 4\eta_{j+1}^n/3 - 5\eta_j^n/2 + 4\eta_{j-1}^n/3 - \eta_{j-2}^n/12),$$

$$(V_j^{n-\frac{1}{2}})_t = -\lambda \frac{|\psi_{j+1}^n|^2 - |\psi_{j-1}^n|^2}{2h}. \tag{2.21}$$

The truncation error of the SRK is of order $(\tau^2 + h^4)$, and the scheme is conditionally stable with a weak stable condition defined by the Runge–Kutta method. It should be note that, unlike the SSS scheme, the proposed SRK can incorporate general boundary conditions such as the Dirichlet or Neumann types.

2.6. Runge–Kutta method with five-point difference (RK5)

Another approach to solve Eq. (1.1) is directly using the Runge–Kutta method. In order to achieve a high accuracy in the space direction, the term $\frac{\epsilon^2}{2}\psi_{xx}^\epsilon$ is discretized by a five-point difference formula in RK5. The resulting discrete difference equations are then solved by the fourth-order accurate RK method. The RK5 scheme is given by

$$\psi_j^{n+1} = \psi_j^n + (K_1 + 2K_2 + 2K_3 + K_4)/6, \tag{2.22}$$
$$K_1 = G(\psi_j^n), \qquad K_2 = G(\psi_j^n + 0.5K_1),$$
$$K_3 = G(\psi_j^n + 0.5K_2), \qquad K_4 = G(\psi_j^n + K_3),$$
$$G(\eta_j^n) = \frac{i\epsilon\tau}{2h^2}\left(-\eta_{j+2}^n/12 + 4\eta_{j+1}^n/3 - 5\eta_j^n/2 + 4\eta_{j-1}^n/3 - \eta_{j-2}^n/12\right) - \frac{i\tau}{\epsilon}\left(\alpha|\eta_j^n|^2 - \alpha + V_j^{n+\frac{1}{2}}\right) \times \eta_j^n,$$
$$(V_j^{n-\frac{1}{2}})_t = -\lambda\frac{|\psi_{j+1}^n|^2 - |\psi_{j-1}^n|^2}{2h}. \tag{2.23}$$

The truncation error of Eq. (2.22) is of order $(\tau^4 + h^4)$. The RK5 scheme is conditionally stable with a weak stable condition given by the Runge–Kutta method.

2.7. Time-splitting spectral methods (BSP1 and BSP2)

Bao et al. [3] recently proposed two time-splitting spectral methods for Eq. (1.1).

1. BSP1

$$\widetilde{\psi}_j^{n+1} = F_j^{-1}\left(e^{-i\tau\epsilon k^2\pi^2/2p^2} \times F_k(\psi_j^n)\right), \tag{2.24}$$
$$\psi_j^{n+1} = e^{-\frac{i\tau}{\epsilon}(\alpha(|\widetilde{\psi}_j^{n+1}|^2 - 1) + V_j^{n+\frac{1}{2}})} \times \widetilde{\psi}_j^{n+1}, \tag{2.25}$$
$$(V_j^{n-\frac{1}{2}})_t = -\lambda\frac{|\psi_{j+1}^n|^2 - |\psi_{j-1}^n|^2}{2h}, \tag{2.26}$$

2. BSP2

$$\bar{\psi}_j^{n+1} = e^{-\frac{i\tau}{2\epsilon}(\alpha(|\psi_j^n|^2 - 1) + V_j^{n+\frac{1}{2}})} \times \psi_j^n, \tag{2.27}$$
$$\widetilde{\psi}_j^{n+1} = F_j^{-1}\left(e^{-i\tau\epsilon k^2\pi^2/2p^2} \times F_k(\bar{\psi}_j^n)\right), \tag{2.28}$$
$$\psi_j^{n+1} = e^{-\frac{i\tau}{2\epsilon}(\alpha(|\widetilde{\psi}_j^{n+1})|^2 - 1) + V_j^{n+\frac{1}{2}})} \times \widetilde{\psi}_j^{n+1}, \tag{2.29}$$
$$(V_j^{n-\frac{1}{2}})_t = -\lambda\frac{|\psi_{j+1}^n|^2 - |\psi_{j-1}^n|^2}{2h}, \tag{2.30}$$

The BSP1 is essentially the same as the SSS scheme reported in Eqs. (2.16)–(2.18). The main difference is in the order of solving the split Eqs. (2.14) and (2.15). Notice that in BSP2, Eq. (2.15) is solved twice. The truncation errors of BSP1 and BSP2 are of order $(\tau^2 + h^m)$, where m denotes the smoothness of the solution. Both BSP1 and BSP2 schemes are unconditionally stable by means of the linearized stability analysis.

Remark. More accurate schemes have been employed to compute Eq. (1.2). However, numerical results using the more accuracy schemes are almost the same as those based on the simple second order scheme for Eq. (2.2). It is also of interest to note that, the Schrödinger equation itself shows the dimensional relation $[t] = [x]^2$, i.e., it has a diffusion scaling. Comparing with the SRK method which has truncation error of order $(\tau^2 + h^4)$, this implies that τ has dimension h^2, $[\tau] = [h]^2$, which is consistent with the Schrödinger equation. This can be regarded as the dimensional analysis's interpretation of the stability analysis.

3. Conservative properties

The long-wave short-wave interaction equations admit certain conservation laws, and they have been reported by Lin and Wong in [19]. For accurate numerical computations, it is important that the numerical schemes presented in the last section also preserve the conservative properties.

Theorem 3.1. *The following conservation properties are held in the CNI scheme* Eqs. (2.1)–(2.5);

$$\|\psi^n\|^2 = \text{const.}, \tag{3.1}$$
$$h\sum_{j=0}^{J} V_j^{n+\frac{1}{2}} = \text{const.}, \tag{3.2}$$
$$h\sum_{j=1}^{J}(V_j^{n-\frac{1}{2}})_t|\psi_j^n|^2 = 0, \tag{3.3}$$
$$E^n = \text{const.}, \tag{3.4}$$

where the energy density E^n is given by

$$E^n = \frac{\epsilon^2}{2}\|\psi_x^n\|^2 + \frac{\alpha}{2}h\sum_{j=1}^{J}(|\psi_j^n|^2-1)^2 + h\sum_{j=1}^{J}V_j^{n-\frac{1}{2}}|\psi_j^n|^2. \tag{3.5}$$

Proof. Computing the inner product of Eq. (2.1) with $(\psi_j^{n+1}+\psi_j^n)$ and taking the imaginary part, we have

$$\mathrm{i}\epsilon\frac{(\psi_j^{n+1}-\psi_j^n,\psi_j^{n+1}+\psi_j^n)}{\tau} + \frac{\epsilon^2}{4}((\psi_j^{n+1}+\psi_j^n)_{x\bar{x}},\psi_j^{n+1}+\psi_j^n) - \left(\left(\alpha\left(\frac{|\psi_j^{n+1}|^2+|\psi_j^n|^2}{2}-1\right)+V_j^{n+\frac{1}{2}}\right)\frac{\psi_j^{n+1}+\psi_j^n}{2},\psi_j^{n+1}+\psi_j^n\right)=0,$$

where

$$\begin{aligned}
&\mathrm{Re}(\psi_j^{n+1}-\psi_j^n,\psi_j^{n+1}+\psi_j^n) = \|\psi^{n+1}\|^2-\|\psi^n\|^2,\\
&\mathrm{Im}\left((\psi_j^{n+1}+\psi_j^n)_{x\bar{x}},\psi_j^{n+1}+\psi_j^n\right) = -\mathrm{Im}((\psi_j^{n+1}+\psi_j^n)_x,(\psi_j^{n+1}+\psi_j^n)_x)=0,\\
&\mathrm{Im}\left(\left(\alpha(\frac{|\psi_j^{n+1}|^2+|\psi_j^n|^2}{2}-1)+V_j^{n+\frac{1}{2}}\right)\frac{\psi_j^{n+1}+\psi_j^n}{2},\psi_j^{n+1}+\psi_j^n\right)\\
&= \mathrm{Im}h\sum_{j=1}^{J}\left(\alpha\left(\frac{|\psi_j^{n+1}|^2+|\psi_j^n|^2}{2}-1\right)+V_j^{n+\frac{1}{2}}\right)\frac{|\psi_j^{n+1}+\psi_j^n|^2}{2}=0.
\end{aligned}$$

Here Im and Re denote the imaginary and real parts of a complex number respectively and the pair $(\cdot,\cdot)$ is the inner product. Thus,

$$\|\psi^{n+1}\|^2 = \|\psi^n\|^2 = \cdots = \|\psi^0\|^2 = \mathrm{const}.$$

Summing up (2.2) for j, it gives

$$\begin{aligned}
h\sum_{j=0}^{J}V_j^{n+\frac{1}{2}} &= h\sum_{j=0}^{J}V_j^{n-\frac{1}{2}} - \frac{\lambda\tau}{2}\left(\sum_{j=0}^{J}|\psi_{j+1}^n|^2-\sum_{j=0}^{J}|\psi_{j-1}^n|^2\right)\\
&= h\sum_{j=0}^{J}V_j^{n-\frac{1}{2}} - \frac{\lambda\tau}{2}\left(\sum_{j=0}^{J}|\psi_j^n|^2-\sum_{j=0}^{J}|\psi_j^n|^2\right)\\
&= h\sum_{j=0}^{J}V_j^{n-\frac{1}{2}} = \cdots = h\sum_{j=0}^{J}V_j^{-\frac{1}{2}} = \mathrm{const.},
\end{aligned}$$

where the boundary condition (2.5) is used. Computing the inner product of Eq. (2.2) with $|\psi_j^n|^2$, it yields

$$h\sum_{j=1}^{J}(V_j^{n-\frac{1}{2}})_t|\psi_j^n|^2 = -\frac{\lambda}{2h}h\sum_{j=1}^{J}(|\psi_{j+1}^n|^2|\psi_j^n|^2|-|\psi_{j-1}^n|^2|\psi_j^n|^2)=0.$$

Finally, computing the inner product of Eq. (2.1) with $(\psi_j^{n+1}-\psi_j^n)$ and taking the real part, we obtain

$$\begin{aligned}
&\mathrm{Re}\left[\frac{\epsilon^2}{4}((\psi_j^{n+1}+\psi_j^n)_{x\bar{x}},\psi_j^{n+1}-\psi_j^n) - \frac{\alpha}{4}(|\psi_j^{n+1}|^2+|\psi_j^n|^2)(\psi_j^{n+1}+\psi_j^n),\psi_j^{n+1}-\psi_j^n)\right.\\
&\left.+\frac{\alpha}{2}(\psi_j^{n+1}+\psi_j^n,\psi_j^{n+1}-\psi_j^n) - \frac{1}{2}h\sum_{j=1}^{J}V_j^{n+\frac{1}{2}}(\psi_j^{n+1}+\psi_j^n)\overline{(\psi_j^{n+1}-\psi_j^n)}\right]=0.
\end{aligned}\tag{3.6}$$

The terms of Eq. (3.6) are computed as follows:

$$\begin{aligned}
&\mathrm{Re}\left[\frac{\epsilon^2}{4}((\psi_j^{n+1}+\psi_j^n)_{x\bar{x}},\psi_j^{n+1}-\psi_j^n)\right] = \mathrm{Re}\left[-\frac{\epsilon^2}{4}((\psi_j^{n+1}+\psi_j^n)_x,(\psi_j^{n+1}-\psi_j^n)_x)\right] = -\frac{\epsilon^2}{4}(\|\psi_x^{n+1}\|^2-\|\psi_x^n\|^2),\\
&\mathrm{Re}\left[-\frac{\alpha}{4}(|\psi_j^{n+1}|^2+|\psi_j^n|^2)(\psi_j^{n+1}+\psi_j^n),\psi_j^{n+1}-\psi_j^n)\right] = -\frac{\alpha}{4}h\sum_{j=1}^{J}(|\psi_j^{n+1}|^4-|\psi_j^n|^4),\\
&\mathrm{Re}\left[\frac{\alpha}{2}(\psi_j^{n+1}+\psi_j^n,\psi_j^{n+1}-\psi_j^n)\right] = \frac{\alpha}{2}h\sum_{j=1}^{J}(|\psi_j^{n+1}|^2-|\psi_j^n|^2),
\end{aligned}$$

$$
\begin{aligned}
&\mathrm{Re}\left[-\frac{1}{2}h\sum_{j=0}^{J}V_j^{n+\frac{1}{2}}(\psi_j^{n+1}+\psi_j^n)\overline{(\psi_j^{n+1}-\psi_j^n)}\right]\\
&=-\frac{1}{2}h\sum_{j=1}^{J}V_j^{n+\frac{1}{2}}(|\psi_j^{n+1}|^2-|\psi_j^n|^2)\\
&=-\frac{1}{2}h\sum_{j=1}^{J}(V_j^{n+\frac{1}{2}}|\psi_j^{n+1}|^2-V_j^{n-\frac{1}{2}}|\psi_j^n|^2)+\frac{1}{2}h\sum_{j=1}^{J}(V_j^{n+\frac{1}{2}}-V_j^{n-\frac{1}{2}})|\psi_j^n|^2\\
&=-\frac{1}{2}h\sum_{j=1}^{J}(V_j^{n+\frac{1}{2}}|\psi_j^{n+1}|^2-V_j^{n-\frac{1}{2}}|\psi_j^n|^2)-\frac{\tau\lambda}{4}\sum_{j=1}^{J}(|\psi_{j+1}^n|^2-|\psi_{j-1}^n|^2)|\psi_j^n|^2\\
&=-\frac{1}{2}h\sum_{j=1}^{J}(V_j^{n+\frac{1}{2}}|\psi_j^{n+1}|^2-V_j^{n-\frac{1}{2}}|\psi_j^n|^2)-\frac{\tau\lambda}{4}\sum_{j=1}^{J}(|\psi_{j+1}^n|^2|\psi_j^n|^2-|\psi_{j-1}^n|^2|\psi_j^n|^2)\\
&=-\frac{1}{2}h\sum_{j=1}^{J}(V_j^{n+\frac{1}{2}}|\psi_j^{n+1}|^2-V_j^{n-\frac{1}{2}}|\psi_j^n|^2),
\end{aligned}
$$

where Eq. (2.2) and the boundary condition (2.5) are applied. Thus, we have from Eq. (3.6) that

$$
-\frac{\epsilon^2}{4}(\|\psi_x^{n+1}\|^2-\|\psi_x^n\|^2)-\frac{\alpha}{4}h\sum_{j=1}^{J}(|\psi_j^{n+1}|^4-|\psi_j^n|^4)+\frac{\alpha}{2}h\sum_{j=1}^{J}(|\psi_j^{n+1}|^2-|\psi_j^n|^2)-\frac{1}{2}h\sum_{j=1}^{J}(V_j^{n+\frac{1}{2}}|\psi_j^{n+1}|^2-V_j^{n-\frac{1}{2}}|\psi_j^n|^2)=0,
$$

i.e.,

$$
\begin{aligned}
\frac{\epsilon^2}{4}\|\psi_x^{n+1}\|^2+\frac{\alpha}{4}h\sum_{j=1}^{J}(|\psi_j^{n+1}|^2-1)^2+\frac{1}{2}h\sum_{j=1}^{J}V_j^{n+\frac{1}{2}}|\psi_j^{n+1}|^2&=\frac{\epsilon^2}{4}\|\psi_x^n\|^2+\frac{\alpha}{4}h\sum_{j=1}^{J}(|\psi_j^n|^2-1)^2+\frac{1}{2}h\sum_{j=1}^{J}V_j^{n-\frac{1}{2}}|\psi_j^n|^2=\cdots=\\
&=\frac{\epsilon^2}{4}\|\psi_x^0\|^2+\frac{\alpha}{4}h\sum_{j=1}^{J}(|\psi_j^0|^2-1)^2+\frac{1}{2}h\sum_{j=1}^{J}V_j^{-\frac{1}{2}}|\psi_j^0|^2=\mathrm{const}.
\end{aligned}
$$

It is clear that the discrete conservation laws presented in Eqs. (3.1)–(3.5) are analogous to the conservation laws given in Eq. 1.5 and (1.7)–(1.10), for which the differential Eqs. (1.1)–(1.4) hold. Therefore, the CNI scheme Eqs. (2.1)–(2.5) preserves the important conservative properties. □

Theorem 3.2. *The 3LE scheme Eqs. (2.8) and (2.9) possesses the discrete conservation laws (3.2) and (3.3) and*

$$
h\sum_{j=1}^{J}\mathrm{Re}(\psi_j^{n+1}\psi_j^n)=\mathrm{const}. \tag{3.7}
$$

Proof. Computing the inner product of Eq. (2.8) with ψ_j^n and by taking the imaginary part, we get Eq. (3.7). The proofs of (3.2) and (3.3) are the same as those already reported in the Theorem 3.1. □

Theorem 3.3. *The HOP scheme* Eqs. (2.11)–(2.13), *the SRK method* Eqs. (2.19)–(2.21), *and the RK5 method* Eqs. (2.22) and (2.23) *satisfy the discrete conservation laws* (3.2) and (3.3).

The proof of this theorem is standard and will be omitted.

Theorem 3.4. *The SSS method* Eqs. (2.16)–(2.18), *time-splitting spectral BSP1* Eqs. (2.24)–(2.26) *and BSP2* Eqs. (2.27)–(2.30) *satisfy the discrete conservation laws* (3.1)–(3.3).

Proof. From Eq. (2.16), it yields

$$
|\widetilde{\psi}_j^{n+1}|=|\psi_j^n|.
$$

By using the Parseval's relation twice, we have

$$
\|\psi^{n+1}\|_2^2=(x_R-x_L)\sum_{k=-\frac{M}{2}}^{\frac{M}{2}-1}(F_k(\widetilde{\psi}_j^{n+1}))^2=h\sum_{j=1}^{J}|\widetilde{\psi}_j^n|^2=\|\psi^n\|_2^2.
$$

Similar deduction shows that the conservation laws (3.1) holds for BSP1 and BSP2. The proofs of (3.2) and (3.3) are the same as those given in the Theorem 3.1. □

Remark. All conservative theorems reported in this section also hold for the homogeneous Dirichlet boundary condition.

4. Plane wave solution

In this section, we consider a special case for the differential system Eqs. (1.1)–(1.4), in which an exact plane wave solution can be derived.

Let

$$\begin{cases} V^{\varepsilon} = d, \\ \psi^{\epsilon} = A\mathrm{e}^{\mathrm{i}(k\pi x/p-\omega t)}, \end{cases} \tag{4.1}$$

where d, A, k and ω are constants. Substituting (4.1) into Eqs. (1.1) and (1.2), it gives

$$\begin{cases} \mathrm{i}\epsilon(-\mathrm{i}\omega)\psi^{\epsilon} + \frac{\epsilon^2}{2}(\mathrm{i}\frac{k\pi}{p})^2\psi^{\epsilon} - (\alpha(A^2-1)+d)\psi^{\epsilon} = 0, \\ V_t^{\epsilon} = -\lambda(|\psi^{\epsilon}|^2)_x = 0. \end{cases} \tag{4.2}$$

It then follows from Eq. (4.2) that

$$\omega = \frac{\frac{\pi^2\epsilon^2k^2}{2p^2} + \alpha A^2 - \alpha + d}{\epsilon}. \tag{4.3}$$

Therefore, if ω satisfies the dispersion relation Eq. (4.3), Eqs. (1.1)–(1.4) has an exact plane wave solution given by Eq. (4.1). Here, we consider the discrete plane wave solution

$$\begin{cases} V_j^n = d, \\ \psi_j^n = A\mathrm{e}^{\mathrm{i}(k\pi jh/p-\omega n\tau)} = Ar^n\mathrm{e}^{\mathrm{i}k\pi jh/p}, \quad r = \mathrm{e}^{-\mathrm{i}\omega\tau}, \quad |r| = 1. \end{cases} \tag{4.4}$$

4.1. Crank–Nicolson implicit scheme

For the CNI scheme, substituting Eq. (4.4) into Eq. (2.1), we have

$$\frac{\mathrm{i}\epsilon}{\tau}Ar^n\mathrm{e}^{\mathrm{i}\frac{k\pi}{p}jh}(r-1) + \frac{\epsilon^2}{4h^2}(\mathrm{e}^{\mathrm{i}\frac{kh\pi}{p}} - 2 + \mathrm{e}^{-\mathrm{i}\frac{kh\pi}{p}})Ar^n\mathrm{e}^{\mathrm{i}\frac{k\pi}{p}jh}(r+1) - (\alpha A^2 - \alpha + d)\frac{r+1}{2}Ar^n\mathrm{e}^{\mathrm{i}\frac{k\pi}{p}jh} = 0 \tag{4.5}$$

which gives

$$r = \frac{\mathrm{i}\epsilon + \frac{\epsilon^2\tau}{h^2}\sin^2\frac{kh\pi}{2p} + \frac{\tau}{2}(\alpha A^2 - \alpha + d)}{\mathrm{i}\epsilon - \frac{\epsilon^2\tau}{h^2}\sin^2\frac{kh\pi}{2p} - \frac{\tau}{2}(\alpha A^2 - \alpha + d)}, \qquad |r| = 1, \tag{4.6}$$

and

$$\begin{aligned} \omega &= \frac{1}{\tau}\arcsin\frac{\tau\left(\frac{2\epsilon^3}{h^2}\sin^2\frac{kh\pi}{2p} + \varepsilon(\alpha A^2 - \alpha + d)\right)}{\epsilon^2 + \tau^2\left(\frac{\epsilon^2}{h^2}\sin^2\frac{kh\pi}{2p} + \frac{1}{2}(\alpha A^2 - \alpha + d)\right)^2} = \frac{\frac{2\epsilon^3}{h^2}\sin^2\frac{kh\pi}{2p} + \epsilon(\alpha A^2 - \alpha + d)}{\epsilon^2 + \tau^2\left(\frac{\epsilon^2}{h^2}\sin^2\frac{kh\pi}{2p} + \frac{1}{2}(\alpha A^2 - \alpha + d)\right)^2} + \mathrm{O}(\tau^2) \\ &= \frac{\frac{\pi^2\epsilon^2k^2}{2p} + \alpha A^2 - \alpha + d}{\epsilon} + \mathrm{O}(\tau^2 + h^2). \end{aligned} \tag{4.7}$$

It is clear that the plane wave solution satisfies the CNI scheme with the error $\mathrm{O}(\tau^2 + h^2)$.

4.2. Three-level explicit scheme

Substituting Eq. (4.4) into Eq. (2.8), we have

$$\frac{\mathrm{i}\epsilon}{2\tau}(r^2-1) + \frac{\epsilon^2}{2h^2}\left(\mathrm{e}^{\mathrm{i}\frac{kh\pi}{p}} - 2 + \mathrm{e}^{-\mathrm{i}\frac{kh\pi}{p}}\right)r - (\alpha A^2 - \alpha + d)r = 0$$

which is equivalent to

$$\mathrm{i}\epsilon r^2 - 2\tau\Lambda r - \mathrm{i}\epsilon = 0 \quad \text{where} \quad \Lambda \equiv \frac{2\epsilon^2}{h^2}\sin^2\frac{kh\pi}{2p} + \alpha A^2 - \alpha + d.$$

Thus

$$r = \frac{-2\mathrm{i}\tau\Lambda \pm \sqrt{-4\tau^2\Lambda^2 + 4\epsilon^2}}{2\epsilon}. \tag{4.8}$$

It follows from (4.8) that $|r| = 1$, if

$$\tau \leqslant \frac{\epsilon}{\Lambda}. \tag{4.9}$$

When the condition (4.9) is satisfied, we get

$$\omega = \frac{1}{\tau}\arcsin\frac{2\tau\Lambda}{2\epsilon} = \frac{\Lambda}{\epsilon} + O(\tau^2) = \frac{\frac{\pi^2\epsilon^2k^2}{2p^2} + \alpha A^2 - \alpha + d}{\epsilon} + O(h^2 + \tau^2). \tag{4.10}$$

Remark. The condition (4.9) holds for any integer $k \geqslant 0$. Thus, it is equivalent to

$$\tau \leqslant \frac{\epsilon}{\Lambda} = \frac{\epsilon}{\frac{2\epsilon^2}{h^2} + \alpha A^2 - \alpha + d}$$

which can be expressed approximately as

$$\tau \leqslant \frac{h^2}{2\epsilon}, \tag{4.11}$$

for h sufficiently small. The condition (4.11) is the linearized stability condition for the three-level scheme.

4.3. Hopscotch Scheme

In the HOP scheme, implicit and explicit steps are carried out alternatively. For a fixed j, the solution is computed by Eq. (2.10) when $n + j$ is even at time step $n + 1$, and then follows by Eq. (2.11) at time step $n + 2$. At the $n + 1$ step, this is equivalent to a three-level scheme given by

$$i\epsilon\frac{\psi_j^{n+1} - \psi_j^{n-1}}{\tau} + \epsilon^2(\psi_j^n)_{x\bar{x}} - 2\left(\alpha\left(\frac{|\psi_{j+1}^n|^2 + |\psi_{j-1}^n|^2}{2} - 1\right) + V_j^{n-\frac{1}{2}}\right)\psi_j^n = 0, \tag{4.12}$$

when $n + j$ is odd. At the $n + 2$ step, the HOP scheme is equivalent to

$$\begin{aligned} &i\epsilon\frac{\psi_j^{n+2} - \psi_j^n}{\tau} + \frac{\epsilon^2}{2}((\psi_j^{n+2})_{x\bar{x}} + (\psi_j^n)_{x\bar{x}}) \\ &- \left(\alpha\left(\frac{|\psi_{j+1}^{n+2}|^2 + |\psi_{j-1}^{n+2}|^2}{2} - 1\right) + V_j^{n+\frac{3}{2}}\right)\psi_j^{n+2} - \left(\alpha\left(\frac{|\psi_{j+1}^n|^2 - |\psi_{j-1}^n|^2}{2} - 1\right) + V_j^{n+\frac{1}{2}}\right)\psi_j^n = 0, \end{aligned} \tag{4.13}$$

when $n + j$ is even.

Substituting Eq. (4.4) into Eqs. (4.12) and (4.13), we have

$$\frac{i\epsilon}{\tau}(r^2 - 1) + \frac{\epsilon^2 r}{h^2}\left(e^{i\frac{kh\pi}{p}} - 2 + e^{-i\frac{kh\pi}{p}}\right) - 2r(\alpha A^2 - \alpha + d) = 0, \tag{4.14}$$

and

$$\frac{i\epsilon}{\tau}(r^2 - 1) + \frac{\epsilon^2}{2h^2}\left(e^{i\frac{kh\pi}{p}} - 2 + e^{-i\frac{kh\pi}{p}}\right)(r^2 + 1) - (\alpha A^2 - \alpha + d)(r^2 + 1) = 0. \tag{4.15}$$

It is noted that only $r = 1$ satisfies Eqs. (4.14) and (4.15) simultaneously. Therefore, the HOP scheme does not admit the plane wave solution.

4.4. Split step spectral method

Using the formulae given in Eqs. (2.14) and (2.15) and the discrete Fourier transform, we have the plane wave solution for the SSS method,

$$\begin{aligned} &\psi_j^n = Ae^{i(\frac{k\pi}{p}jh - \omega n\tau)}, \\ &\widetilde{\psi}_j^{n+1} = Ae^{-\frac{i\tau}{\epsilon}(\alpha A^2 - \alpha + d) + i\frac{k\pi}{p}jh - i\omega n\tau}, \\ &F_l(\widetilde{\psi}_j^{n+1}) = A\frac{1}{M}\sum_{j=-\frac{M}{2}}^{\frac{M}{2}-1}\widetilde{\psi}_j^{n+1}e^{-\frac{2\pi ijl}{M}} = \begin{cases} 0, & l \neq k, \\ Ae^{-i\tau(\frac{\alpha A^2 - \alpha + d}{\epsilon} + \omega n)}, & l = k, \end{cases} \end{aligned}$$

where $M = \frac{2p}{h}$ and

$$\psi_j^{n+1} = A e^{\frac{-i\tau\epsilon k^2\pi^2}{2p^2}} e^{-i\tau\left(\frac{\alpha A^2-\alpha+d}{\epsilon}+\omega n\right)} e^{\frac{2\pi i j k}{M}}.$$

This is equal to the plane wave solution at the $n+1$ time step, i.e.,

$$\psi_j^{n+1} = A e^{i\left(\frac{k\pi j h}{p}-\omega(n+1)\tau\right)}.$$

Thus, we get

$$-i\omega(n+1)\tau = -\frac{i\tau\epsilon k^2\pi^2}{2p^2} - i\tau\left(\frac{\alpha A^2-\alpha+d}{\epsilon}+\omega n\right),$$

i.e.,

$$\omega = \frac{\frac{\pi^2\epsilon^2 k^2}{2p^2}+\alpha A^2-\alpha+d}{\epsilon}. \tag{4.16}$$

Therefore, the SSS scheme admits the exact plane wave solution, which is consistent with the high accuracy of the SSS scheme.

4.5. Split step Runge–Kutta method

Substituting (4.4) into (2.19) and (2.20), we get

$$\begin{aligned}
&\widetilde{\psi}_j^{n+1} = A e^{-\frac{i\tau}{\epsilon}(\alpha A^2-\alpha+d)} r^n e^{ij\frac{k\pi h}{p}},\\
&\psi_j^{n+1} = \widetilde{\psi}_j^{n+1} + \frac{1}{6}(K_1+K_2+K_3+K_4),\\
&K_1 = G(\widetilde{\psi}_j^{n+1}) = \frac{i\epsilon\tau}{3h^2}\widetilde{\psi}_j^{n+1}\left(-8\sin^2\frac{k\pi h}{2p}+\frac{1}{2}\sin^2\frac{k\pi h}{p}\right) \equiv q\widetilde{\psi}_j^{n+1},\\
&K_2 = G\left(1+\frac{q}{2}\widetilde{\psi}_j^{n+1}\right) = \left(1+\frac{q}{2}\right)q\widetilde{\psi}_j^{n+1},\\
&K_3 = \left(1+\frac{q}{2}(1+\frac{q}{2})\right)q\widetilde{\psi}_j^{n+1},\\
&K_4 = \left(1+q\left(1+\frac{q}{2}\left(1+\frac{q}{2}\right)\right)\right)q\widetilde{\psi}_j^{n+1}.
\end{aligned}$$

Combining the formulae, implies

$$\psi_j^{n+1} = \widetilde{\psi}_j^{n+1}\left(1+q\left(\left(1+\frac{q}{6}+\frac{q}{6}\left(1+\frac{q}{2}\right)+\frac{q}{6}\left(1+\frac{q}{2}\left(1+\frac{q}{2}\right)\right)\right)\right)\right).$$

Using the Taylor's expansion, we have

$$8\sin^2\frac{k\pi h}{2p}-\frac{1}{2}\sin^2\frac{k\pi h}{p} = \frac{3}{2}\frac{k^2\pi^2h^2}{p^2}+O(h^6)$$

which gives

$$q = -\frac{i\tau\epsilon k^2\pi^2}{2p^2}+O(h^4).$$

Thus,

$$\psi_j^{n+1} = \widetilde{\psi}_j^{n+1}\left(1-\frac{i\tau\epsilon k^2\pi^2}{2p^2}+O(h^4)\right)$$

and

$$r = e^{-\frac{i\tau}{\epsilon}(\alpha A^2-\alpha+d)}\left(1-\frac{i\tau\epsilon k^2\pi^2}{2p^2}+O(\tau^2+h^4)\right),$$

from which we have

$$\omega = \frac{\frac{\pi^2\epsilon^2k^2}{2p}+\alpha A^2-\alpha+d}{\epsilon}+O(\tau^2+h^2). \tag{4.17}$$

The plane wave solution satisfies the SRK method with the error $O(\tau^2+h^4)$.

4.6. Runge–Kutta Method with five-point difference

Similar to the deduction for the SRK method, the RK5 Scheme Eqs. (2.22) and (2.23) satisfies

$$\omega = \frac{\frac{\pi^2\epsilon^2k^2}{2p} + \alpha A^2 - \alpha + d}{\epsilon} + O(\tau^2 + h^4), \tag{4.18}$$

i.e., the plane wave solution holds with the error $O(\tau^2 + h^4)$.

4.7. Time-splitting spectral methods

It follows from the deduction for the SSS method that

$$\omega = \frac{\frac{\pi^2\epsilon^2k^2}{2p} + \alpha A^2 - \alpha + d}{\epsilon}. \tag{4.19}$$

The plane wave solution satisfies exactly the time-splitting spectral methods BSP1 and BSP2.

Remark. From the analysis of the plane wave solution, we note that the order of accuracy of the the numerical schemes are the same as those of the truncation errors of the corresponding schemes. In the 3LE scheme, the condition for the existence of the plane wave solution is the same as that required for the stability. The truncation error of the HOP scheme is $O\left(\tau^2 + h^2 + \frac{\tau^2}{h^2}\right)$ and may be $O(1)$ for general step sizes in space and time. Hence, no plane wave solution is expected for the HOP scheme. The analysis of the plane wave solution presented in this section serves as a useful tool for testing the numerical schemes.

5. Case studies

To validate the proposed computational schemes for the long-wave short-wave interaction equations, we consider the following case studies. In order to compare the numerical solutions with the known exact solutions, we first consider cases when the initial condition $V_0^\epsilon(x)$ in Eq. (1.4) is a constant, such that $V_0^\epsilon(x) = d$. Taking $\lambda = 0$ in Eq. (1.2), the long-wave solution remains constant with $V^\epsilon(x,t) = d$. Here, we focus on the initial condition for the short-wave given by

$$\psi_0^\epsilon(x) \equiv A_0(x)\exp\left(\frac{\mathrm{i}}{\epsilon}S_0(x)\right),$$

with the following choices for $A_0(x)$ and $S_0(x)$.

5.1. Initial data of plane wave with weak $O(\epsilon)$ cubic defocusing nonlinearity

For the plane wave solution discussed in Section 4, the initial data is chosen as:

$$A_0(x) = A, \quad S_0(x) = \frac{\epsilon k\pi x}{p}.$$

The exact solution is then given by

$$\psi^\epsilon(x,t) = A\exp\left(\mathrm{i}\left(\frac{k\pi x}{p} - \omega t\right)\right), \tag{5.1}$$

where ω is defined in Eq. (4.3). In performing the computation, we use the following values for the parameters:

$$A = 2, \qquad K = 1, \qquad P = 5, \qquad d = 1 \qquad \alpha = 1.$$

5.2. Initial data of plane wave with strong $O(1)$ cubic defocusing nonlinearity

We consider a stronger plane wave and the initial data given by

$$A_0(x) = A, \quad S_0(x) = \frac{k\pi x}{p}.$$

The exact solution is

$$\psi^\epsilon(x,t) = A\exp\left(\mathrm{i}\left(\frac{k\pi x}{\epsilon p} - \omega t\right)\right), \tag{5.2}$$

where

$$\omega = \frac{\frac{\pi^2 k^2}{2p^2} + \alpha A^2 - \alpha + d}{\epsilon}$$

In performing the computation, we use the following values for the parameters:

$$A = 2, \qquad K = 1, \qquad P = 5, \qquad d = 1 \qquad \alpha = 1.$$

5.3. Initial data of the soliton

Next, we consider a soliton solution for Eqs. (1.1)–(1.4). It is easy to verify that the soliton solution

$$\psi^{\epsilon}(x,t) = \operatorname{sech}(c_0 x + c_1 + c_2 t)\exp(-\mathrm{i}(c_3 x + c_4 + c_5 t)), \tag{5.3}$$

satisfies the following equations:

$$\begin{cases} \epsilon c_3 c_0 - c_2 = 0, \\ \epsilon^2 c_0^2 + \alpha = 0, \\ c_5 - \frac{\epsilon}{2} c_0^2 - \frac{\epsilon}{2} c_3^2 - \frac{d}{\epsilon} = 0. \end{cases} \tag{5.4}$$

Hence, we let the initial value be

$$A_0(x) = \operatorname{sech}(c_0 x + c_1), \quad S_0(x) = -\epsilon(c_3 x + c_4), \tag{5.5}$$

and the constants be taken as

$$c_0 = \frac{1}{\sqrt{\epsilon}}, \qquad c_1 = 2, \qquad c_2 = -4, \qquad c_3 = -\frac{-4}{\sqrt{\epsilon}}, \qquad c_4 = 2c_3, \qquad c_5 = \frac{17}{2} + \frac{1}{\epsilon}, \qquad \alpha = -\epsilon.$$

In addition to the three cases with exact solutions, we also consider the following initial data which have been commonly chosen for the long-wave short-wave equations.

5.4. Zero initial phase data

Let

$$A_0(x) = \mathrm{e}^{-x^2}, \qquad S_0(x) = 0. \tag{5.6}$$

This is very similar to the purely soliton data reported early by Miller and Kamvissis [22], where

$$A_0(x) = 2\operatorname{sech}(x), \qquad S_0(x) = 0.$$

For the data set considered in [22], the Zakharov–Shabat operator has purely imaginary eigenvalues and the reflection coefficients are exactly zero. For the present data, the eigenvalues are almost purely imaginary and the reflection coefficients are exponentially small for small ϵ.

5.5. Symmetric initial data with nonzero phase

Let

$$A_0(x) = \frac{\sinh(2x)}{\cosh^2(2x)}, \qquad S_0(x) = \frac{1}{\cosh(2x)}. \tag{5.7}$$

The eigenvalues generated by this data have been studied numerically by Bronski [8]. The eigenvalues are symmetric about the pure imaginary axis, and they are located roughly on a convex"parabola" whose vertex is at the origin. The top of the "parabola" are at the points $0.5 - i$ and $0.5 + i$, Thus, an eigenvalue has a large real part if it has also a large imaginary part, and the eigenvalues have distinct real parts.

5.6. Nonsymmetric initial data

Let

$$A_0(x) = \frac{1}{\cosh(2x)}, \qquad S_0(x) = \frac{2x}{\cosh(2x)}. \tag{5.8}$$

This example lacks the even/odd symmetry possessed by the initial data given in III and IV. Moreover, the eigenvalues are not right/left symmetric [6].

5.7. Non-analytic initial data

Let

$$A_0(x) = \begin{cases} 1-|x| & \text{if} \quad |x|<1, \\ 0 & \text{otherwise}, \end{cases} \qquad S_0(x) = \frac{1}{\cosh(2x)}. \tag{5.9}$$

Notice that this initial data is not analytic at $x = 0$ and $x = \pm 1$.

Remark. In this section, all initial data are given in the interval $[-p, +p]$, where $L = 2p$ is the length of the computational domain. But, in actual computational, the interval is re-scaled to $[0, L]$.

6. Numerical experiments

In this section, we investigate the accuracy and the efficiency of various numerical schemes. First, the numerical algorithms are tested for Cases I–III for which the corresponding exact solutions are known. The computed solutions are compared using the approach reported in [9]. Namely we fix the accuracy (L_∞) from $t = 0$ to $t = T$ and let the step sizes h and τ vary. For each scheme, the step sizes are chosen such that the numerical solution is stable and the least computing time to attain a given accuracy is recorded. The CPU in second is based on a PC Pentium computer, and the efficiency of various algorithms can be compared from the reported computing time.

Table 1
Comparison of various schemes for the plane wave solution Eq. (5.1)

Method	ϵ	Step size	Time (s)	L_∞^p	L_∞^v	E_1	E_2
CNI	1.0	$h = 1.25\tau = .03$	2.65 (−4)	1.57(−2)	8.62(−7)	1.17(−6)	2.13(−6)
	0.1	$h = 2.5\tau = .0015$	2.28(−3)	1.58(−2)	1.78(−7)	8.89(−7)	1.19(−6)
	0.01	$h = 2\tau = .00005$	7.81(−2)	1.62(−2)	3.12(−5)	6.85(−5)	1.26(−4)
	0.001	$h = 2.5\tau = .0000007$	4.92(0)	9.46(−3)	9.29(−11)	1.72(−6)	3.25(−6)
3LE	1.0	$h = 2\tau = .06$	1.56 (−5)	1.81(−2)	6.70(−8)	1.70(−3)	3.09(−3)
	0.1	$h = 2.5\tau = .001$	6.25(−4)	6.96(−3)	8.78(−12)	4.47(−7)	8.42(−7)
	0.01	$h = 2.5\tau = .00004$	1.56(−2)	1.65(−2)	1.35(−14)	8.27(−7)	1.55(−6)
	0.001	$h = 2.5\tau = .0000006$	9.06(−1)	4.04(−3)	0.0	1.62(−5)	3.06(−5)
HOP	1.0	$h = 1.25\tau = .0004$	6.09 (−3)	1.82(−2)	1.58(−4)	3.92(−3)	7.09(−3)
	0.1	$h = 2.5\tau = .000001$	1.31(0)	1.98(−2)	1.71(−7)	8.02(−4)	1.50(−3)
	0.01	$h = \tau =$	*				
SSS	1.0	$h = 2.5\tau = .5$	9.38 (−6)	0.0	0.0	8.39(−9)	1.52(−8)
	0.1	$h = 2.5\tau = .5$	9.38(−6)	0.0	0.0	4.72(−8)	8.87(−8)
	0.01	$h = 2.5\tau = .5$	9.38(−6)	0.0	0.0	8.41(−9)	1.58(−8)
	0.001	$h = 2.5\tau = .5$	9.38(−6)	1.19(−7)	0.0	8.86(−8)	1.66(−7)
	0.0001	$h = 2.5\tau = .5$	9.38(−6)	1.19(−7)	0.0	6.91(−8)	1.30(−7)
	0.00001	$h = 2.5\tau = .5$	9.38(−6)	0.0	0.0	4.81(−8)	9.06(−7)
SRK	1.0	$h = 2.5\tau = .5$	5.78 (−6)	1.07(−2)	0.0	0.0	0.0
	0.1	$h = 2.5\tau = .5$	5.78(−6)	1.07(−3)	0.0	0.0	0.0
	0.01	$h = 2.5\tau = .5$	5.78(−6)	1.16(−4)	0.0	0.0	0.0
	0.001	$h = 2.5\tau = .5$	5.78(−6)	6.48(−5)	0.0	0.0	0.0
	0.0001	$h = 2.5\tau = .5$	5.78(−6)	1.01(−3)	0.0	0.0	1.67(−6)
	0.00001	$h = 2.5\tau = .5$	5.78(−6)	1.01(−2)	0.0	0.0	0.0
RK5	1.0	$h = 2\tau = .1$	3.13 (−5)	1.66(−2)	2.20(−8)	1.40(−4)	2.55(−4)
	0.1	$h = 2.5\tau = .006$	4.68(−4)	1.47(−2)	1.66(−10)	4.04(−5)	7.61(−5)
	0.01	$h = 2.5\tau = .0004$	7.81(−3)	8.91(−3)	3.69(−7)	1.02(−4)	1.93(−4)
	0.001	$h = 2.5\tau = .000005$	5.93(−1)	1.80(−2)	2.29(−14)	5.00(−7)	9.41(−7)
BSP1	1.0	$h = 2.5\tau = .5$	9.38(−6)	1.19(−7)	0.0	6.84(−8)	1.24(−7)
	0.1	$h = 2.5\tau = .5$	9.38(−6)	5.87(−7)	0.0	5.16(−8)	9.72(−8)
	0.01	$h = 2.5\tau = .5$	9.38(−6)	8.11(−6)	0.0	1.97(−8)	3.71(−8)
	0.001	$h = 2.5\tau = .5$	9.38(−6)	3.89(−5)	0.0	5.69(−9)	1.07(−8)
	0.0001	$h = 2.5\tau = .5$	9.38(−6)	3.83(−6)	0.0	6.58(−8)	1.23(−7)
	0.00001	$h = 2.5\tau = .5$	9.38(−6)	4.05(−7)	0.0	4.30(−8)	8.11(−8)
BSP2	1.0	$h = 2.5\tau = .5$	1.09(−5)	1.19(−7)	0.0	5.16(−8)	9.40(−8)
	0.1	$h = 2.5\tau = .5$	1.09(−5)	1.19(−7)	0.0	6.21(−8)	1.16(−7)
	0.01	$h = 2.5\tau = .5$	1.09(−5)	9.70(−6)	0.0	9.36(−8)	1.76(−7)
	0.001	$h = 2.5\tau = .5$	1.09(−5)	3.81(−5)	0.0	4.20(−8)	7.92(−8)
	0.0001	$h = 2.5\tau = .5$	1.09(−5)	1.72(−3)	0.0	5.29(−8)	9.97(−8)
	0.00001	$h = 2.5\tau = .5$	1.09(−5)	6.65(−3)	0.0	2.44(−8)	4.60(−8)

The computing time corresponds to CPU required to reach $L_\infty < 0.02$ from $t = 0$ to $t = 0.5$.

Throughout the computation, the conservation errors are closely monitored, and they are defined by $E_1 = \frac{(H_1^n - H_1^0)}{H_1^0}$ and $E_2 = \frac{(H_2^n - H_2^0)}{H_2^0}$, where $H_1^n = \|\psi^n\|_{l_2}^2$ and $H_2^n = h\sum_{j=1}^{J}(V_j^{n-\frac{1}{2}})_t|\psi_j^n|^2$. For cases with known exact solutions, we define the solution errors as $L_\infty^p = \max_j|\psi_j^n - \psi(x_j,t^n)|$ and $L_\infty^v = \max_j|V_j^n - V(x_j,t^n)|$, where $\psi(x_j,t^n)$ and $V(x_j,t^n)$ are the exact solutions at the point (x_j,t^n).

In Tables 1–3, we report the computations applied to the plane wave and soliton models, respectively. Particular attention is focused on the accuracy of various numerical schemes, the errors in the L_∞ norm and the conservative quantities given in Eqs. (3.1) and (3.3) are reported. Figs. 1 and 2 illustrate the exact solutions for Cases I and III and with $\epsilon = 1$ and 0.00001. Here, " 1.57(−2)" denotes 1.57×10^{-2}, and " * " indicates the solution fails to reach the given accuracy within 1000 CPU seconds.

Table 2
Comparison of various schemes for the strong defocusing nonlinearity Eq. (5.2)

Method	ϵ	Step size	Time (s)	L_∞^p	L_∞^v	E_1	E_2
SRK	1.0	$h = 2.0\tau = .5$	1.37 (−5)	9.50(−3)	9.81(−8)	2.33(−8)	4.11(−8)
	0.1	$h = 0.125\tau = .06$	1.73(−3)	1.61(−2)	1.38(−7)	7.69(−7)	1.39(−6)
	0.01	$h = .005\tau = .0018$	1.39(0)	4.32(−3)	2.15(−6)	3.49(−8)	6.68(−8)
BSP1	1.0	$h = 2.5\tau = .5$	1.87 (−5)	7.63(−7)	4.27(−8)	1.45(−7)	5.31(−7)
	0.1	$h = .3125\tau = .1$	1.39(−3)	7.87(−3)	1.10(−7)	9.77(−7)	2.01(−8)
	0.01	$h = 0.0195\tau = .01$	1.87(−1)	7.72(−3)	3.54(−6)	1.91(−8)	3.47(−8)

The computing time corresponds to CPU required to reach $L_\infty < 0.02$ from $t = 0$ to $t = 1.0$.

Table 3
Comparison of various schemes for the soliton solution Eq. (5.3)

Method	ϵ	Step size	Time (s)	L_∞^p	L_∞^v	E_1	E_2
CNI	1.0	$h = .02\tau = .006$	2.81 (−1)	9.28(−3)	0.0	6.65(−7)	8.05(−7)
	0.1	$h = .0035\tau = .0035$	2.90(0)	8.90(−3)	0.0	6.23(−6)	3.61(−5)
	0.01	$h = .0003\tau = .0003$	5.72(2)	9.56(−3)	0.0	5.02(−5)	8.53(−5)
	0.001	$h = \tau =$	*				
3LE	1.0	$h = .025\tau = .0003$	7.03 (−1)	8.74(−3)	0.0	8.93(−3)	2.38(−7)
	0.1	$h = .008\tau = .0003$	2.21(0)	8.89(−3)	0.0	2.01(−7)	1.27(−6)
	0.01	$h = .0035\tau = .0002$	3.47(1)	9.39(−3)	0.0	1.52(−7)	2.82(−7)
	0.001	$h\tau$	*				
HOP	1.0	$h = \tau =$					
SSS	1.0	$h = .3125\tau = .05$	3.13 (−3)	7.95(−3)	0.0	2.19(−6)	7.54(−4)
	0.1	$h = .078\tau = .05$	1.56(−2)	7.97(−3)	0.0	1.73(−6)	7.87(−4)
	0.01	$h = .039\tau = .04$	3.12(−2)	6.15(−3)	0.0	3.19(−6)	6.97(−5)
	0.001	$h = .0097\tau = .05$	1.09(−1)	8.01(−3)	0.0	2.51(−6)	6.19(−6)
	0.0001	$h = .0024\tau = .05$	4.21(−1)	7.89(−3)	0.0	2.56(−6)	2.88(−6)
	0.00001	$h = 6.10(-4)\tau = .05$	1.87(0)	7.71(−3)	0.0	3.17(−7)	2.28(−7)
SRK	1.0	$h = .12\tau = .015$	1.11(−2)	9.24(−3)	0.0	1.02(−5)	8.80(−5)
	0.1	$h = .038\tau = .015$	3.53(−2)	9.28(−3)	0.0	1.00(−5)	1.75(−4)
	0.01	$h = .012\tau = .015$	1.13(−1)	9.24(−3)	0.0	1.03(−5)	2.44(−5)
	0.001	$h = .0038\tau = .015$	3.06(−1)	9.30(−3)	0.0	1.01(−5)	1.23(−5)
	0.0001	$h = .0012\tau = .015$	1.03(0)	9.26(−3)	0.0	1.03(−5)	1.08(−5)
	0.00001	$h = .000385\tau = .016$	2.99(0)	9.61(−3)	0.0	1.40(−5)	1.42(−5)
RK5	1.0	$h = .1\tau = .01$	3.12 (−2)	4.35(−3)	0.0	2.14(−6)	1.59(−5)
	0.1	$h = .03\tau = .008$	9.38(−2)	3.59(−3)	0.0	2.25(−5)	1.66(−4)
	0.01	$h = .01\tau = .002$	6.93(0)	5.80(−3)	0.0	7.24(−4)	1.34(−3)
	0.001	$h = .0033\tau = .00015$	1.41(2)	8.79(−3)	0.0	1.10(−3)	1.31(−3)
BSP1	1.0	$h = .3125\tau = .05$	3.13 (−3)	8.07(−3)	0.0	2.64(−6)	8.05(−4)
	0.1	$h = .078\tau = .05$	1.56(−2)	8.02(−3)	0.0	1.98(−6)	8.72(−4)
	0.01	$h = .039\tau = .04$	3.12(−2)	8.25(−3)	0.0	3.07(−6)	4.95(−5)
	0.001	$h = .0097\tau = .05$	1.09(−1)	8.07(−3)	0.0	2.76(−6)	2.16(−6)
	0.0001	$h = .0024\tau = .05$	4.21(−1)	8.96(−3)	0.0	2.98(−6)	3.51(−6)
	0.00001	$h = 6.10(-4)\tau = .05$	1.87(0)	8.19(−3)	0.0	2.66(−6)	2.69(−6)
BSP2	1.0	$h = .3125\tau = .05$	3.87 (−3)	6.16(−4)	0.0	2.03(−6)	1.54(−5)
	0.1	$h = .078\tau = .05$	2.05(−2)	3.91(−4)	0.0	2.10(−6)	5.94(−6)
	0.01	$h = .039\tau = .04$	3.84(−2)	3.65(−3)	0.0	3.28(−6)	1.22(−5)
	0.001	$h = .0097\tau = .05$	1.25(−1)	3.51(−4)	0.0	2.82(−6)	3.25(−6)
	0.0001	$h = .0024\tau = .05$	5.16(−1)	3.44(−4)	0.0	2.57(−6)	2.71(−6)
	0.00001	$h = 6.10(-4)\tau = .05$	2.28(0)	1.34(−3)	0.0	2.66(−6)	2.70(−6)

The computing time corresponds to CPU required to reach $L_\infty < 0.02$ from $t = 0$ to $t = 1.0$.

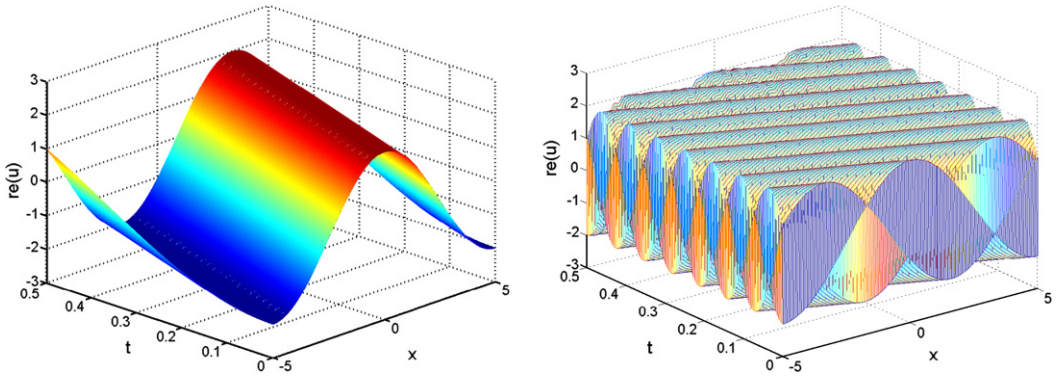

Fig. 1. Real parts of the plane wave solution (Case I), $\epsilon = 1$ (left) and $\epsilon = 0.00001$ (right).

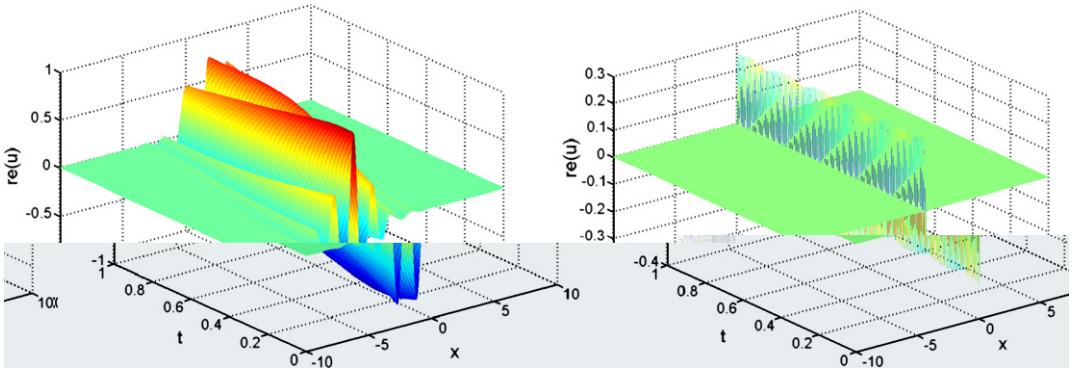

Fig. 2. Real Parts of the Soliton Solution, $\epsilon = 1$ (left) and $\epsilon = 0.00001$ (right).

From the computational results presented for Case I, we note that all numerical schemes except the HOP are capable of solving the plane wave solutions for $\epsilon = 1.0, 0.1, 0.01$ and 0.001. It has been shown that the HOP does not admit the plane wave solution in Section 4.3, and this remark is confirmed by the numerical simulation. For the plane wave solution with a strong cubic defocusing nonlinearity Case II, the computation becomes more difficult as the parameter ϵ is decreasing. In Table 2, we compare only the SRK and BSP1 schemes for $\epsilon = 1, 0.1, 0.01$. For the soliton solution reported in Table 3, the CNI, 3LE and HOP methods fail when ϵ is very small. RK5 method can be applied to both Cases I and III, but small step sizes are required as ϵ is decreasing. Hence, we conclude that for efficient computations especially for cases with a strong nonlinearity, a split step algorithm such as the SSS, SRK, BSP1 and BSP2 should be employed. In general, we expect that the mesh sizes are chosen to be $h = O(\epsilon)$ and $\tau = (\epsilon)$. The results in Tables 1 and 3 indicate that even as ϵ is decreasing, the time step τ is almost constant. However, τ is more sensitive for systems with a strong defocusing nonlinearity. Since the spectral based algorithms have higher order of accuracy, in particularly in the space direction, smaller mesh sizes are required for the SRK scheme.

Among the various split step schemes, the performance in terms of accuracy and computing time are comparable. Hence, Table 4 only presents the computations based on SSS and SRK for Cases IV–VII, the results using BSP1 and BSP2 are comparable to those based on SSS. In Fig. 3, the imaginary Parts for Case IV for $\epsilon = 1$ and $\epsilon = 0.00001$ are displayed. The SRK is capable of providing accurate solutions as the spectral based methods for a wide range of ϵ, and the time step is not sensitive with the variation of the value of ϵ. It is of interest to note that the SRK requires less CPU time when ϵ is small. For Cases IV–VII with $\epsilon = 0.00001$, the improvement of the computing time based on the SRK compared with those reported by the SSS method are 31%, 84%, 149% and 58%, respectively. From Fig. 4, we observe that better symmetry is preserved using the SRK (bottom left) than the SSS (top right).

In the SRK scheme, it is crucial to employ a high order method such as the five-point difference to approximate the term ψ_{xx}. Table 5 compares the performance when the three-point finite-difference is used instead of the five-point formula for Case III – soliton solutions. It is clear that when a low order approximation is used in SRK, much smaller step sizes in space and times are required to ensure the stability for all values of ϵ. Consequently, the computing time deteriorates significantly.

Notice that, by multiplying Eq. (1.1) with $\overline{\psi^\epsilon}$ and taking the imaginary part, we have

Table 4
Computational results for Cases IV–VII and $\alpha = 1.0$

Method	Model	ϵ	Step size	Time (s)	E_1	E_2
SSS	III	1.0	$h = .3125\tau = .1$	.0012	6.70(−7)	0.0024
		0.00001	$h = .0048\tau = .01$	.9565	1.28(−5)	3.20(−4)
	IV	1.0	$h = .3125\tau = .1$	.0012	1.12(−6)	6.15(−4)
		0.00001	$h = .0048\tau = .005$	1.91	2.55(−5)	2.59(−6)
	V	1.0	$h = .4687\tau = .1$	.0012	7.09(−7)	6.25(−3)
		0.00001	$h = .0073\tau = .005$	1.93	2.55(−5)	9.19(−6)
	VI	1.0	$h = .4687\tau = .1$	.0012	9.10(−7)	6.44(−3)
		0.00001	$h = .0073\tau = .005$	1.97	2.55(−5)	5.58(−6)
SRK	III	1.0	$h = .2\tau = .04$	.0027	2.22(−6)	9.51(−4)
		0.00001	$h = .005\tau = .008$	.7315	1.34(−8)	1.08(−4)
	IV	1.0	$h = .16\tau = .025$	.0051	5.66(−4)	6.38(−4)
		0.00001	$h = .004\tau = .005$	1.036	3.16(−8)	8.34(−7)
	V	1.0	$h = .2\tau = .04$	.0040	2.25(−3)	4.58(−3)
		0.00001	$h = .005\tau = .008$	.7751	2.76(−8)	5.34(−5)
	VI	1.0	$h = .2\tau = .04$	.0084	4.71(−3)	8.40(−3)
		0.00001	$h = .004\tau = .005$	1.25	4.04(−8)	2.84(−5)

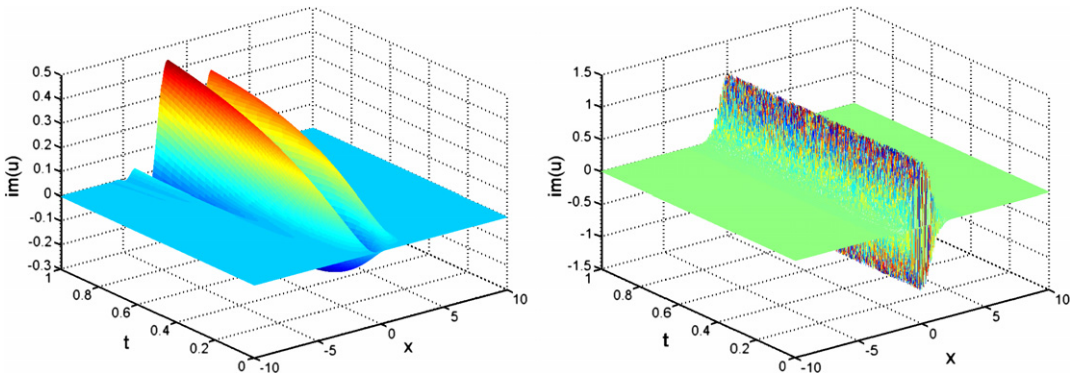

Fig. 3. Imaginary Parts for Case IV, $\epsilon = 1$ (left) and $\epsilon = 0.00001$ (right).

$$2(|\psi^\epsilon|^2)_t + \mathrm{Im}\left(\frac{\epsilon}{2}\psi^\epsilon_{xx}\overline{\psi^\epsilon}\right) = 0.$$

The value of the $|\psi^\epsilon|^2$ at each point varies slowly with time for small ϵ, which is illustrated in Fig. 4 for Case V. The profile of $|\psi^\epsilon|^2$ is changing with time when $\epsilon = 1$ (Fig. 4, top left), but the variation is almost unnoticeable when $\epsilon = 0.00001$ (Fig. 4, top right and bottom left). However, the real part (Fig. 4, bottom right) and the imaginary part of the solutions oscillate rapidly. In the computation, it suffices to reduce the step size in space with ϵ, while the time step can keep constant. Since the nonlinearity is weaker for small value of ϵ, it leads to a slow variation of $|\psi^\epsilon|^2$ and a weak diffusion term $\epsilon(\psi^\epsilon)_{xx}$. Consequently, from the computational point of view, it is not difficult to deal with problems of strong cubic defocusing nonlinearity with small parameter of ϵ. The SSS, SRK, BSP1 and BSP2 methods have also been successfully tested for non-symmetry and non-analytical initial data (Cases VI and VII), but we will not report these results due to the page limitation.

Finally, we demonstrate that the SRK and the spectral based schemes can be used to compute general long-wave short-wave interaction equations, i.e., the initial condition for $V_0^\epsilon(x) = d$ is not a constant. Here, we only present the results based on the SRK scheme, and consider a test case given as follows.

Bounded state solutions of (1.1) and (1.2) are, by definition, solutions of the form

$$\psi^\epsilon(x,t) = \mathrm{e}^{\mathrm{i}\omega t} f(x - ct), \qquad V^\epsilon(x,t) = g(x - ct), \tag{6.1}$$

where f and g are functions which vanish at infinity in some sense, and ω and c are real constants. For a more precise definition of the bounded sate or the ground-state solutions, it means that $(\psi^\epsilon, V^\epsilon)$ minimizes the Hamiltonian functional of (1.1) and (1.2). However, we will not discuss the detail in this section, readers interested in this topic are referred to [1,17].

Substituting (6.1) into Eqs. (1.1) and (1.2) leads to the following system of ordinary differential equations for f and g

$$\frac{\epsilon^2}{2}f'' - \mathrm{i}\epsilon c f' - [\alpha f^2 - (\alpha - \epsilon\omega) + g]f = 0, \tag{6.2}$$

$$-cg' = -\lambda(|f|^2)'. \tag{6.3}$$

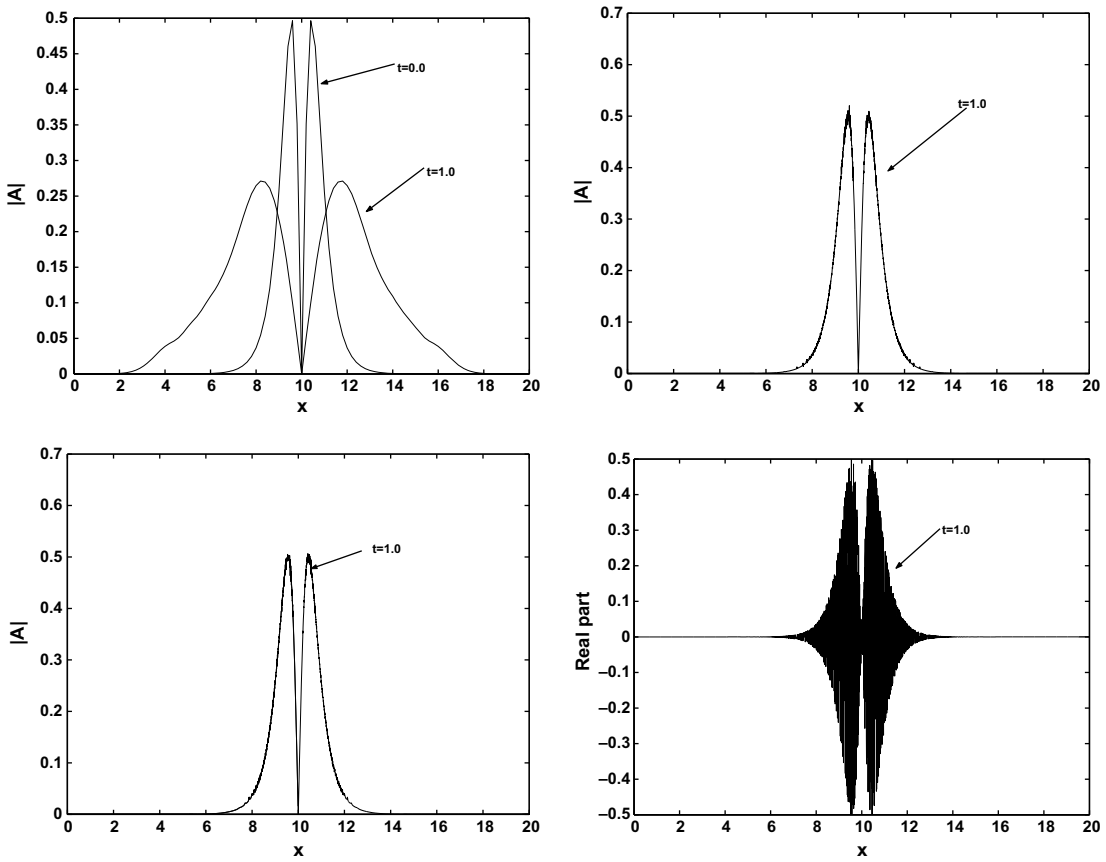

Fig. 4. Case V, SSS results $\epsilon = 1$ (top left); $\epsilon = 0.00001$ (top right); SRK results $\epsilon = 0.00001$, (bottom left);and Real part of solution of model V, $\epsilon = 0.00001$ (bottom right).

We then deduce from (6.3) that

$$g = \frac{\lambda}{c}|f|^2 \tag{6.4}$$

except for a possible constant. Setting $F(x) = e^{-\frac{icx}{\epsilon}} f(x)$, we find that F satisfies the following ordinary differential equation

$$\epsilon^2 F'' - a|F|^2 F - bF = 0, \tag{6.5}$$

where

$$a = -2\left(\alpha + \frac{c}{\lambda}\right), \qquad b = 2(c^2 + \epsilon\omega - \alpha).$$

This equation occurs in the study of the ground-state solution of the cubic nonlinear Schrödinger equation. When $b > 0$, F can be computed explicitly

$$F(x) = \sqrt{\frac{2b}{|a|}}\frac{1}{\cosh\left(\frac{\sqrt{b}}{\epsilon}x\right)} = \sqrt{\frac{2b}{|a|}}\operatorname{sech}\left(\frac{\sqrt{b}}{\epsilon}x\right). \tag{6.6}$$

Therefore $f(x) = e^{\frac{icx}{\epsilon}}F(x + x_0)$ and $g(x) = G(x + x_0)$ where x_0 is a real number and

$$G(x) = \frac{\lambda}{c}\frac{2b}{|a|}\operatorname{sech}^2\left(\frac{\sqrt{b}}{\epsilon}x\right). \tag{6.7}$$

As has been studied in [19], the zero-dispersion limit or the semi-classical limit of the long-wave short-wave interaction Eqs. (1.1) and (1.2) is similar to the cubic nonlinear Schrödinger equation. Basically the short-wave wave plays more role than the long wave. Although it does not show explicitly in the limit equation, indeed, the long-wave changes the initial data in the semi-classical limit. To understand this phenomenon and the zero-dispersion limit of the associated ground-state

Table 5
Comparison of SRK with three-point and five-point difference for Case III.

Method	ϵ	Step size	Time (s)	L^p_∞	L^v_∞	E_1	E_2
Three-point	1.0	$h = .025\tau = .0008$	1.34 (0)	8.73(−3)	0.0	2.48(−7)	1.05(−6)
	0.1	$h = .008\tau = .0008$	4.31(0)	8.96(−3)	0.0	1.36(−7)	2.20(−7)
	0.01	$h = .0025\tau = .0008$	1.40(1)	8.75(−3)	0.0	1.65(−7)	1.92(−8)
	0.001	$h = .0008\tau = .0009$	4.28(1)	8.96(−3)	0.0	3.66(−9)	3.30(−9)
	0.0001	$h = .00025\tau = .0008$	1.42(2)	8.75(−3)	0.0	2.87(−7)	3.82(−9)
	0.00001	$h = .00008\tau = .0009$	4.18(2)	7.32(−3)	0.0	5.58(−8)	5.67(−8)
Five-point	1.0	$h = .12\tau = .015$	1.11(−2)	9.24(−3)	0.0	1.02(−5)	8.80(−5)
	0.1	$h = .038\tau = .015$	3.53(−2)	9.28(−3)	0.0	1.00(−5)	1.75(−4)
	0.01	$h = .012\tau = .015$	1.13(−1)	9.24(−3)	0.0	1.03(−5)	2.44(−5)
	0.001	$h = .0038\tau = .015$	3.06(−1)	9.30(−3)	0.0	1.01(−5)	1.23(−5)
	0.0001	$h = .0012\tau = .015$	1.03(0)	9.26(−3)	0.0	1.03(−5)	1.08(−5)
	0.00001	$h = .000385\tau = .016$	2.99(0)	9.52(−3)	0.0	1.01(−5)	1.03(−5)

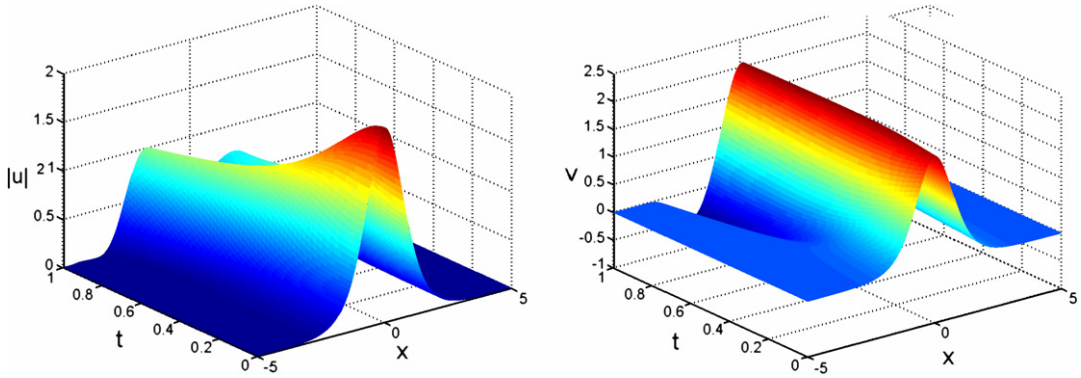

Fig. 5. $|u|^2$ (left) and V (right) of the bounded state solution for $\epsilon = 1$.

solution, we present numerical simulations with initial data related to the bound-state solutions. In particular, we consider the cases when $\epsilon = 1$ and $\epsilon = 0.001$ in order to see the small dispersion effect. In Fig. 5, we choose the bounded state initial conditions $u_0(x) = \sqrt{2}/\cosh(x)$, $V_0(x) = 2/[\cosh(x)]^2$. In this case, for large dispersion $\epsilon = 1$, the oscillation occurs only when the time becomes large for real and imaginary parts of u. The oscillation is due to the dispersive nature of the short-wave. However, $|u|^2$ is well behaved because of the conservation of density. Numerical simulations show that both $|u|^2$ and the long-wave V look like a soliton for a while; at least before the splitting of the profile occurs, and the profiles are related and agreed with the theoretical prediction of the bound state solution. In Fig. 6, we consider the small dispersion case, $\epsilon = 0.001$, with the same bounded state initial conditions $u_0(x) = \sqrt{2}/\cosh(x)$, $V_0(x) = 2/[\cosh(x)]^2$. In this case, for a short time, both real and imaginary parts of the short-wave u oscillate strongly. However, $|u|^2$ and V still behave well, and we observe peaks appear in the long-wave as time increases. Although the long-wave V satisfies the conservation law equation, one will expect it should behave like a soliton wave. But as investigated in [19], the long-wave will affect the short-wave

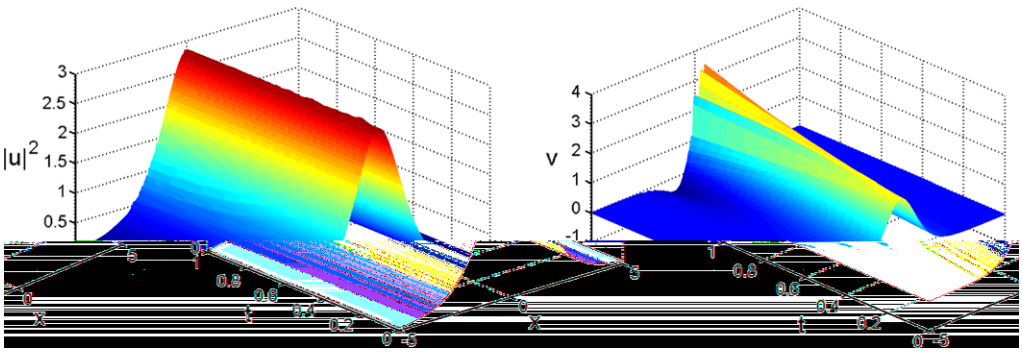

Fig. 6. $|u|^2$ (left) and V (right) of the bounded state solution for $\epsilon = 0.001$.

for a weak coupling in the zero-dispersion limit. Therefore, it will be an interesting and challenging problem to investigate the existence of the spike solutions in the long-wave–short-wave equations when the dispersion is small for the strong coupling cases. For a smaller dispersion, say $\epsilon = 0.00001$ for example, computations can be carried out, but the numerical solutions are too chaotic to provide any detail structure. We would like to mention that although the short-wave u oscillates strongly, the wave packet remains stable and it is expected to be well-behaved by using a suitable averaging.

Various numerical schemes are studied for the long-wave short-wave interaction equations. It has been demonstrated that split step approach with spectral based algorithms is an efficient way to solve the coupled system numerically. In addition to the standard spectral methods, we introduce a novel SRK scheme which is based on a time-splitting approach combined with the Runge–Kutta algorithm. The most attractive feature of the proposed SRK scheme is that it does not require the application of a discrete Fourier transform. Not only do we observe that the computing time is comparable for most test cases with small ϵ, the SRK can directly apply to problems with general boundary conditions, while a periodic boundary condition is required in a spectral method. Since the SRK scheme does not require the use of discrete Fourier transforms, from the computational point of view, it may be even more efficient when dealing with problems in two and three dimensions.

Acknowledgments

We would like to thank Professor Tang Tao, Professor W.-Z. Bao and the referees for their valuable comments and suggestions leading to the improvement of the manuscript. Q.S. Chang and C.K. Lin would like to thank the Department of Mathematics & Statistical Science, University of Alberta for the hospitality during their stay. This research was supported in part by the Natural Sciences and Engineering Research Council of Canada. The research of CKL was also supported in part by National Science Council of Taiwan under the Grant 95-2115-M-009-MY3 and 5-500 of College of Science, NCTU.

References

[1] J. Albert, J.A. Pava, Existence and stability of ground-state solutions of a Schrödinger-KdV system, Proc. Royal Soc. Edinburgh 133 (2003) 987–1029.
[2] W. Bao, S. Jin, P.A. Markowich, On time-splitting spectral approximation for the Schroedinger equation in the semiclassical regime, J. Comput. Phys. 175 (2002) 487–524.
[3] W. Bao, S. Jin, P.A. Markowich, Numerical study of time-splitting spectral discretizations of nonlinear Schrödinger equations in the semiclassical regimes, SIAM J. Sci. Comput. 23 (2003) 27–64.
[4] W. Bao, N.J. Mauser, H.P. Stimming, Effective one particle quantum dynamics of electrons: a numerical study of the Schrödinger–Poisson-X_α model, Commun. Math. Sci. 1 (2003) 809–828.
[5] W. Bao, C. Zheng, A time-splitting spectral method for three-wave interactions in media with competing quadratic and cubic nonlinearities, Commun. Comput. Phys. 2 (2007) 123–140.
[6] D. Bekiranov, T. Ogawa, G. Ponce, Interaction equation for short and long dispersive waves, J. Funct. Anal. 158 (1998) 357–388.
[7] D.J. Benney, A general theory for interactions between short and long waves, Stud. Appl. Math. 56 (1977) 81–94.
[8] J.C. Bronski, Semiclassical eigenvalue distribution of the Zakharov–Shabat eigenvalue problem, Physica D 97 (1996) 376–397.
[9] Q. Chang, E. Jia, W. Sun, Difference schemes for solving the generalized nonlinear Schrödinger equation, J. Comput. Phys. 184 (1999) 397–415.
[10] Q. Chang, B. Guo, H. Jiang, Finite difference method for generalized Zakharov equations, Math. Comput. 64 (1995) 537–553.
[11] Q. Chang, L. Xu, A numerical method for a system of generalized nonlinear Schrödinger equations, J. Comput. Math. 4 (1986) 191–199.
[12] T. Colin, D. Lannes, Long-wave short-wave resonance for nonlinear geometric optics, Duke Math. J. 107 (2001) 351–419.
[13] B. Desjardins, C.K. Lin, T.C. Tso, Seniclassical limit of the derivative nonlinear Schrödinger equation, Math. Models Meth. Appl. Sci. 10 (2000) 261–285.
[14] B. Desjardins, C.K. Lin, On the semiclassical limit of the general modified NLS equation, J. Math. Anal. Appl. 260 (2001) 546–571.
[15] V.D. Djordjevic, L.G. Redekopp, On two-dimensional packets of capillary-gravity waves, J. Fluid Mech. 79 (1977) 703–714.
[16] S. Jin, C.D. Levermore, D.W. McLaughlin, The semiclassical limit of the defocusing NLS hierarchy, Commun. Pure Appl. Math. 52 (1999) 613–654.
[17] P. Laurencot, On a nonlinear Schrödinger equation arising in the theory of water wave, Nonlinear Anal., Theory, Meth. Appl. 24 (1995) 509–527.
[18] J.H. Lee, C.K. Lin, The behavior of solutions of NLS equation of derivative type in the semiclassical limit, Chaos, Solitons Fract. 13 (2002) 1475–1492.
[19] C.K. Lin, Y.S. Wong, Zero-dispersion limit of the short-wave–long-wave interaction equations, J. Differ. Equations 228 (2006) 87–110.
[20] P.A. Markowich, P. Pietra, C. Pohl, Numerical approximation of quadratic observables of Schrödinger-type equations in the semi-classical limit, Numer. Math. 81 (1999) 595–630.
[21] P.A. Markowich, P. Pietra, C. Pohl, H.P. Stimming, A Wigner-measure analysis of the Dufort–Frankel scheme for the Schrödinger equation, SIAM J. Numer. Anal. 40 (2002) 1281–1310.
[22] P.D. Miller, S. Kamvissis, On the semiclassical limit of the focusing nonlinear Schrödinger equations, Phys. Lett. A 247 (1998) 75–86.
[23] T. Ogawa, Global well-posedness and conservation laws for the water wave interaction equation, Proc. Royal Soc. Edinburgh 127A (1997) 368–384.
[24] N. Sepulveda, Solitary waves in the resonant phenomenon between a surface gravity wave packet and internal gravity wave, Phys. Fluids 30 (1987) 1984–1992.
[25] T.R. Taha, M.J. Ablowitz, Analytical and numerical aspects of certin nonlinear evolution equations, II. Numerical nonlinear Schrödinger equation, J. Comput. Phys. 55 (1984) 203.
[26] M. Tsutsumi, S. Hatano, Well-posedness of the Cauchy problem for the long wave–short wave resonance equations, Nonlinear Anal., Theory, Meth. Appl. 24 (1994) 155–171.
[27] Y.S. Wong, Q. Chang, L. Gong, An initial-boundary value problem of a nonlinear Klein–Gordon equation, Appl. Math. Comput. 84 (1997) 77–93.